AGU PUBLICATIONS

Journal of Advances in Modeling Earth Systems

RESEARCH ARTICLE
10.1002/2015MS000476

A multilevel ocean mixed layer model resolving the diurnal cycle: Development and validation

Tiejun Ling[1], Min Xu[2,3], Xin-Zhong Liang[2,4], Julian X. L. Wang[5], and Yign Noh[6]

[1]Key Laboratory of Research on Marine Hazards Forecasting, National Marine Environmental Forecasting Center, Beijing, China, [2]Earth System Science Interdisciplinary Center, University of Maryland, College Park, Maryland, USA, [3]Now in Climate Change Science Institute, Oak Ridge National Laboratory, Oak Ridge, Tennessee, USA, [4]Department of Atmospheric and Oceanic Science, University of Maryland, College Park, Maryland, USA, [5]Air Resources Laboratory, National Oceanic and Atmospheric Administration, College Park, Maryland, USA, [6]Department of Atmospheric Sciences, Global Environmental Laboratory, Yonsei University, Seoul, South Korea

Key Points:
- The upper ocean mixed layer model developed based on TKE closure model
- The numerical improvements focus on simulating surface temperature better
- The model reproduces sea surface and skin temperature diurnal cycle very well

Correspondence to:
X.-Z. Liang,
xliang@umd.edu

Citation:
Ling, T., M. Xu, X.-Z. Liang, J. X. L. Wang, and Y. Noh (2015), A multilevel ocean mixed layer model resolving the diurnal cycle: Development and validation, *J. Adv. Model. Earth Syst.*, *7*, 1680–1692, doi:10.1002/2015MS000476.

Received 24 APR 2015
Accepted 17 AUG 2015
Accepted article online 19 AUG 2015
Published online 30 OCT 2015

Abstract The representation of transient air-sea interactions is critical to the prediction of the sea surface temperature diurnal cycle and daily variability. This study develops a multilevel upper ocean model to more realistically resolve these interactions. The model is based on the one-dimensional turbulence kinetic energy closure developed by *Noh et al.* [2011], and incorporates new numerical techniques and improved schemes for model physics. The primary improvements include: (1) a surface momentum flux penetration scheme to better depict velocity shear in the diurnal mixed layer; (2) a solar penetration scheme to improve the penetration of visible and near-infrared bands of solar radiation into the mixed layer ocean; (3) a scheme to resolve the cool-skin and warm-layer effects on sea skin temperature; (4) a vertical grid stretch scheme to achieve higher near-surface resolution with fewer vertical levels; (5) a trapezoidal time integration scheme for flexible time steps; (6) a relaxation term of the previous daily mean difference between observed and modeled sea surface temperature. According to the numerical experiments based on the TOGA-COARE IMET mooring buoy data and the validation by observations from the National Data Buoy Center, NOAA, the results indicate that the new upper ocean mixed layer model improves the simulation of the diurnal cycle of SST and sea skin temperature, especially in amplitude.

1. Introduction

The air-sea interaction is crucial to the climate system. Exchanges of momentum, heat, and mass between the atmosphere and ocean directly impact on the ocean mixed layer. Ocean models often use constant profiles to represent the temperature and salinity of the mixed layer. However, in a snapshot view, the upper ocean is constructed by overlaying several sublayers developed at different temporal scales, including the diurnal, synoptic, and seasonal cycles. It is known that reasonable simulation of the sea surface temperature (SST) diurnal cycle helps reproduce seasonal variation [*Chen et al.*, 1994; *Li et al.*, 2001; *Clayson and Chen*, 2002; *Bernie et al.*, 2005; *Mosedale et al.*, 2005; *Vitart et al.*, 2007]. Despite this, many coupled atmosphere-ocean models still exchange variables only once every several hours, which may not simulate the SST diurnal cycle well, as it may underestimate its amplitude. Thus, even models with higher coupling frequency still contain biases in SST and hence also in surface fluxes, cloud, and surface radiation [*Bernie et al.*, 2007, 2008; *Woolnough et al.*, 2007; *Seo et al.*, 2014]. Even now, ocean mixed layer models with realistic SST diurnal cycles are not extensively used in coupled climate models. Thus, the SST diurnal cycle's effect on climate has not been studied effectively [*Noh et al.*, 2011].

Numerous ocean mixed layer models have been developed and their performances have been validated against large-eddy simulations or observations [*Martin*, 1985; *Kraus*, 1988; *Kantha and Clayson*, 1994]. These models fall into three general categories: (1) bulk models that treat the whole mixed layer as a uniform column with given temperature and velocity profiles; (2) multilayer threshold models that use Richardson numbers or other stability factors to parameterize the mixing [*Price et al.*, 1986; *Chen et al.*, 1994; *Plueddemann and Weller*, 1999]; (3) multilayer turbulence models that solve the turbulence closure equations with parameterized Reynolds stress and turbulence dissipation rates. Some models in this final category directly solve equations of turbulence flux [*Mellor and Yamada*, 1982] or turbulence kinetic energy (TKE) [*Gaspar et al.*, 1990],

while others parameterize the vertical structure of the turbulence fluxes [*Large et al.*, 1994; *Kukulka et al.*, 2013].

In the bulk models, the eddy coefficients are assumed to be infinite within the mixed layer and to be zero below, and the deepening rate of the mixed layer depth cannot be negative. Thus, the mixed layer prognostic equations are simplified to the mixed layer depth diagnostic equations. Bulk mixed layer models save computing resources and are easy to implement. However, they cannot represent the process of the turbulent mixing within and below the mixed layer as well as turbulence multilayer models.

Most ocean multilayer turbulence models are originally derived from the atmosphere planetary boundary models. However, they use different physics mechanisms, especially when the surface heat flux is stabilizing [*Large et al.*, 1994; *Noh*, 1996]. This means that oceanic boundary layer models should not be developed in the same way as atmospheric boundary layer models. Many ocean models tend to show a much stronger shear and temperature gradient within the mixed layer, which contradicts the observed uniform profiles of temperature and velocity [*Noh and Kim*, 1999].

Therefore, this study aims to develop a more reliable ocean mixed layer model to reproduce the SST diurnal cycle. Several methods are applied to improve an ocean mixed layer model [*Noh et al.*, 2011] that has previously performed well in both ideal and real case studies. Section 2 gives a brief introduction to the TOGA-COARE IMET buoy observations on which all experiments are based, and introduces data from the NOAA National Data Buoy Center (NDBC) buoys for model validation. Section 3 describes the *Noh et al.* [2011] model and gives a brief overview of our improvements and experiments. The result, discussions, and model validation are described in section 4. Finally, a summary, conclusion, and prospects for the study's future application are given in section 5.

2. Observations

2.1. IMET Mooring

From October 1992 to March 1993, the Tropical Ocean Global Atmosphere Coupled Ocean-Atmosphere Response Experiment (TOGA COARE) collected multiplatform measurements of oceanic and atmospheric properties during an intensive observing period. The experiment covered a large region of the Pacific Warm Pool. The upper ocean of the pool has weak surface currents and small horizontal temperature and salinity gradients. As a result, it is a good place to study the ocean surface diurnal cycle that is generally affected by vertical mixing processes rather than by horizontal advection [*Weller and Anderson*, 1996; *Feng et al.*, 2000]. Many studies have used these measurements to analyze and model intraseasonal variations and the SST diurnal cycle in this region [*Anderson et al.*, 1996; *Sui et al.*, 1997; *Clayson and Kantha*, 1999; *Chou et al.*, 2000; *Ohlmann and Siegel*, 2000; *Clayson and Chen*, 2002; *Weller et al.*, 2004; *Bernie et al.*, 2005; *Shinoda*, 2005].

This study uses the TOGA data from the Improved Meteorological Instrument (IMET) on board the Woods Hole Oceanographic Institution (WHOI) mooring in the TOGA intensive flux array (IFA) located at 1°45′S, 156°E. These data include: (1) WHOI IMET mooring subsurface data [*Plueddemann et al.*, 1993] with hourly temperature, salinity, and horizontal velocity at 41 vertical levels. The thickness of each layer varies: ∼0.5 m from the surface to a depth of 3 m, ∼2 m at depths of 6–35 m, and ∼10 m at depths below 40 m; (2) IMET buoy-flux data [*Weller and Anderson*, 1996], which includes hourly latent heat, sensible heat, net longwave and shortwave radiation, east and north wind stress components, and sea surface skin temperature (TSK). Also used are the observed standard surface meteorological variables, including rainfall, air temperature, wind, relative humidity, surface pressure, and SST.

Numerous studies have demonstrated the excellent quality and application values of the IMET buoy data. In particular, several modeling works performed simulations of the whole observation period (∼133 days). These include investigations of the precipitation impacts on salinity biases [*Li et al.*, 1998], the overestimation of air-sea feedbacks due to errors in surface air temperature and humidity [*Clayson and Chen*, 2002], the model performance in intraseasonal and diurnal variability [*Bernie et al.*, 2005], and the role of the average diurnal cycle in modulating intraseasonal SST variations [*Shinoda and Hendon*, 1998].

2.2. NDBC Buoys

The National Data Buoy Center [*Hamilton*, 1986] website provides both real time and historical observational data from hundreds of buoys around the world. These include standard meteorological data, continuous

winds, and solar radiation. This study uses as input the hourly standard meteorological observations including wind direction and speed, sea level pressure, SST, air and dewpoint temperatures, and solar radiation flux. The mixed layer model developed below requires additional inputs of surface wind stress, latent and sensible heat fluxes, and net longwave radiation, which were calculated using the surface parameterization schemes from the Climate-Weather Research and Forecasting model CWRF [*Liang et al*., 2012] as driven by the available NDBC data. There were 6152 SST diurnal cycles derived from the observations of 42 buoys along the U.S. coastal oceans between 2007 and 2012. About 55% of these have a SST diurnal amplitude larger than 0.5°C, and about 27% greater than 1°C. These serve as high-quality data resources for an independent test of the performance of the model developed here.

3. The Model and Improvements

3.1. Model Basics

This study is based on a second-order turbulence model of *Noh et al*. [2011]. The model was originally developed by *Noh and Fernando* [1991]. Subsequent improvements include parameterizations of eddy viscosity and TKE flux [*Noh*, 1996; *Noh and Kim*, 1999; *Noh et al*., 2002, 2004, 2011], resulting in a model that agreed well with large eddy simulation (LES) results and observations. Like bulk models, the model can reproduce a uniform mixed layer, but it uses eddy diffusivity and viscosity similar to the Mellor-Yamada model [*Mellor and Yamada*, 1982]. The eddy viscosity and diffusivity are calculated empirically by the velocity scale and length scale of turbulence, respectively. The model's fundamental equations are the prognostic equations of mean velocity, potential temperature, salinity, and TKE. The model shows a certain amount of success simulating SST and TSK diurnal warming under strong and weak wind conditions [*Noh et al*., 2011], but could not reproduce large SST diurnal amplitude well. This study aims to further improve the performance, especially in the representation of diurnal amplitude.

3.2. Improvements

3.2.1. Momentum Penetration

Surface air dynamics generate mixing of the sea surface and subsurface. The modeling community uses two approaches to represent the impact of surface momentum flux on TKE vertical structure. The first approach applies wind stress only to the topmost model layer, and is commonly used in *z*-coordinate models. The second approach applies wind stress to the whole ocean mixed layer, and is commonly used in bulk models.

In a K-profile parameterization (KPP) model, *Zhang and Zebiak* [2002] introduced a simple scheme to penetrate momentum flux into the whole mixed layer. Assuming that wind stress is a body force applied to the entire mixed layer, the momentum flux can be distributed vertically as:

$$\tau = \tau_s(1 - z/h) \tag{1}$$

where h is the mixed layer depth, z is the vertical height from 0 to h, and τ_s the wind stress at the surface. The stress penetrating to level z is applied as an additional force to the mean velocity prognostic equations. Thus, the momentum flux is redistributed in several layers so that stirring in the topmost model layer is weaker and keeps stratification more stable.

3.2.2. Solar Penetration

The SST diurnal cycle is very sensitive to incident solar radiation on the sea surface and subsurface depended on solar penetration in different spectral bands. It is not easy to estimate solar penetration accurately, due to instrument orientation issues [*Colbo and Weller*, 2009] and the radiation transmission dependencies on upper ocean chlorophyll concentration, cloud amount, and solar zenith angle [*Ohlmann and Siegel*, 2000]. Because single decay-scale formulation for solar subsurface heating is not accurate for optical depths within 10 m [*Murtugudde et al*., 2002; *Ohlmann*, 2003; *Kara et al*., 2004], double exponential formulation $(1-A)e^{-z/d1} + Ae^{-z/d2}$ (e.g., classical water types [*Jerlov*, 1976] formulation) was implemented in high-resolution models, where A is the fraction of total radiance for wavelength band 1, and d1 and d2 are reciprocal of the absorption coefficient for solar wavelength band 1 and 2. However, Jerlov water type schemes are obsolete for depicting upper ocean turbidity [*Ohlmann and Siegel*, 2000]. To replace the Jerlov water type II penetrating scheme in *Noh et al*., [2011], this study introduces a two-band time-varying solar

penetration scheme [*Kara et al*., 2005] with more accurate attenuation in 0–20 m depth range. The algorithm of that scheme is briefly described in the Appendix A.

3.2.3. Cool-Skin Temperature

TSK is the temperature at the interface of air and sea, while conventional SST represents the bulk temperature at a depth ranging from several dozen centimeters to several meters. With a high emissivity close to 1, the ocean is considered an excellent "blackbody," so that longwave radiation is directly proportional to the fourth power of the skin temperature. The skin layer is the molecular boundary between the turbulent atmosphere and the turbulent ocean. Incorrect specification of the surface boundary condition leads to errors in estimating latent and sensible heat flux. The cool-skin and the warm-layer beneath affect the sea temperature diurnal cycle in the mixed layer. To account for this effect, *Zeng and Beljaars* [2005] developed a prognostic TSK scheme that depicts the diurnal cycle of both the cool-skin and the warm-layer well. The scheme predicts TSK changes from longwave and shortwave radiation, latent heat, wind stress, and background SST. It includes 12 equations, the details of which are described by *Zeng and Beljaars* [2005].

3.2.4. Previous Daily Mean SST Nudging

A one-dimensional model cannot represent horizontal and vertical advection terms, which inevitably causes long-term climate drift (see a brief discussion in the section 4.2.7). To contain the drift, this study adds a relaxation term to the top layer of the temperature prognostic equation:

$$\frac{1}{\lambda}(\overline{T}_{obs}-\overline{T_1}) \tag{2}$$

where $\overline{T}_{obs}$ and $\overline{T_1}$ are the daily mean observed SST and the modeled top-layer temperature of the previous day, respectively, and λ is the relaxation time, here set to 8640 s. In practice, the modeled top-layer temperature can be relaxed to use the observed SST averaged over a certain period prior to the prediction time. Since SST nudging would induce artificial stratification near the sea surface during the daytime when the temperature gradient is big, here the nudging is only turned on at night. $\overline{T}_{obs}$ can be well defined from buoy data, and also easily obtained from remote sensing. With global satellite retrievals of daily SST, the model improved here can be applied to study the SST diurnal variation continuously in wider spatial and longer temporal coverage.

3.2.5. Vertical Grid Stretch

High vertical resolution is required to represent the several meters of the upper ocean in order to capture the SST diurnal cycle. To reduce the number of model levels for efficient computing without degrading resolution in the near-surface layers, this study introduced a vertical grid stretch scheme [*Mcwilliams et al*., 1990], a second-order vertical discretization scheme with a centered difference operator. The vertical coordinate is formulated as

$$z(k)=\frac{D}{\lambda}\log\left(1-(k-1)\frac{D}{N_z}(1-e^{\lambda})\right) \tag{3}$$

where $z(k)$ is the middle depth of model layer k; D is the maximum mixed layer depth, N_z is the number of model levels, and λ is an adjustable parameter for the stretching. This study sets $D = 150$ m, $N_z = 30$, and $\lambda = -5$. As a result, the thickness of the first layer is 1 m, and it stretches from 2 m at a depth of 20 to ~10 m at a depth of 50 m.

3.2.6. Semi-implicit Time Integration

A trapezoidal semi-implicit time integration scheme was implemented for an accurate but more efficient solution. The scheme discretizes variable A's integration equation $\partial A/\partial t = F(A)$ as

$$(A^{n+1}-A^{n-1})/\Delta t=(1-\beta)F(A^{n+1})+\beta F(A^{n}) \tag{4}$$

where *F(A)* means the function of *A*, and β is a tunable coefficient. Setting $\beta = 0.5$ leads to the Crank-Nicolson scheme, which was used in *Noh et al*. [2011], whereas setting $\beta = 0$ yields the backward implicit scheme. Sensitivity tests showed that $\beta \geq 0.5$ could limit the time step less than 100 s before the result became unreasonable. However, using $\beta \leq 0.4$, the model can allow a time step varying from 120 to 600 s without a significant difference in results from the configuration with $\beta = 0.5$ and a 60 s time step. The mean absolute differences of modeled SST for $\Delta t = 60$, 120, 360, 480, and 600 s are all smaller than 0.084°C.

3.3. Experiments

Five experiments were conducted to investigate the effects of introducing the improvements outlined in section 3.2. The control experiment (CTL) uses the model as originally presented by *Noh et al*. [2011]. The

subsequent sensitivity experiments employ the modified model that consecutively incorporates incremental improvements of the momentum penetration (EXP1), the solar radiation penetration (EXP2), the cool-skin temperature (EXP3), and finally the numerical algorithm combining the daily SST nudging, the vertical grid stretch with $N_z = 30$, and the semi-implicit time integration with $\beta = 0.4$ and $\Delta t = 120$ s (EXP4). In experiments CTL and EXP1–3, the model adopts the original configuration with 150 levels, $\beta = 0.5$, and $\Delta t = 60$ s.

CTL, EXP1, and EXP2 were first conducted under ideal case experiments to demonstrate the fundamental improvements to momentum and solar penetration. Then these experiments were driven by the IMET data described in section 2.1, simulating the TOGA COARE conditions in the tropics, to comprehensively demonstrate all the improvements mentioned in the previous paragraph. The final model, incorporating all these improvements (listed in section 3.2), was independently evaluated on its ability to simulate U.S. coastal conditions in the extratropics using NDBC data (described in section 2.2).

4. Results and Discussions

Solar radiation and wind play a dominant role in the SST diurnal cycle. The solar radiation diurnal cycle is the primary cause of diurnal variation, while turbulent mixing induced by wind stress prevents thermal stratification and reduces diurnal variation. Therefore, a key task during the development of an ocean mixed layer model for simulating SST diurnal variation is to realistically simulate heat and momentum fluxes between the atmosphere and ocean. As mentioned in section 1, large SST diurnal amplitudes are commonly underestimated. The purpose of this study is first to generate better stratification for larger SST diurnal amplitudes by modifying solar and momentum penetration schemes to keep more heat content and less turbulence in top model levels. Second, this study aims to more realistically simulate the TSK diurnal cycle by implementing a scheme with both cool-skin and warm-layer effects. SST nudging at night was implemented to minimize the impact of advection on the model. Furthermore, a grid stretch scheme and semi-implicit time integration were applied to improve model computational efficiency and numerical stability. The numerical results and comparison were analyzed to examine the performance of these improvements.

4.1. Ideal Case Experiments

Following the experiment of *Noh et al*. [2011] investigating the mixed layer model's response to idealized surface heating, this study compares the evolution of CTL, EXP1, and EXP2 temperature profiles under diurnally varying surface heating, $H = H_0[1 - \cos(2\pi t/T)]$ with $H_0 = 350\,\mathrm{W\,m^{-2}}$ and $T = 12$ h, for both weak and strong wind speed ($U = 2$ and $8\,\mathrm{m\,s^{-1}}$) at 10 m above sea surface. When the wind is weak ($U = 2\,\mathrm{m\,s^{-1}}$), a strong temperature gradient appears within 5 m of the surface without a distinct uniform mixed layer (shown in Figures 1a, 1c, and 1e). However, EXP1 and EXP2 warm obviously faster than CTL. When ΔSST reaches the peak of the diurnal cycle, EXP1 shows 0.2°C (12%) SST increase and EXP2 shows 0.5°C (30%) increase over CTL (Figure 1g). When the wind is strong ($U = 8\,\mathrm{m\,s^{-1}}$), the uniform mixed layer is formed and its depth reaches about 10 m (Figures 1b, 1d, and 1f). In this case, EXP1 and EXP2 do not show a great change in ΔSST than CTL, and are not significantly different from each other (Figure 1h). Thus, as the momentum penetrates down, the wind stress is redistributed from the surface to the full depth of the mixed layer. The stability of the entire depth increases because the shear between layers becomes weaker. The improvement to the solar penetration scheme successfully increases SST faster under weak wind conditions. However, CTL, EXP1, and EXP2 show no significant differences under strong wind conditions.

4.2. IMET Buoy Experiments

4.2.1. Control Experiment

CTL uses a vertical resolution of 1 m (and so 150 levels) and a time step of 60 s. Following *Phillips* [1966], the model is initialized with the constant profiles of salinity as 35.2 psu and a logarithmic function of water depth is set for initial ocean currents. The initial temperature of the upper 40 levels varies from 29.5°C to 28.6°C according to observations, and is fixed at 28.6°C from the fortieth level to the bottom.

Considering that the temperature does not change linearly or drastically with depth when the diurnal thermocline is formed [*Kawai and Wada*, 2007], the average sea temperatures at 0.55 and 1.1 m represent observed SST in this study. Figures 2a and 2b shows that the model reproduces SST evolution during the whole period without a significant drift. The model captures the observed SST variations very well on days

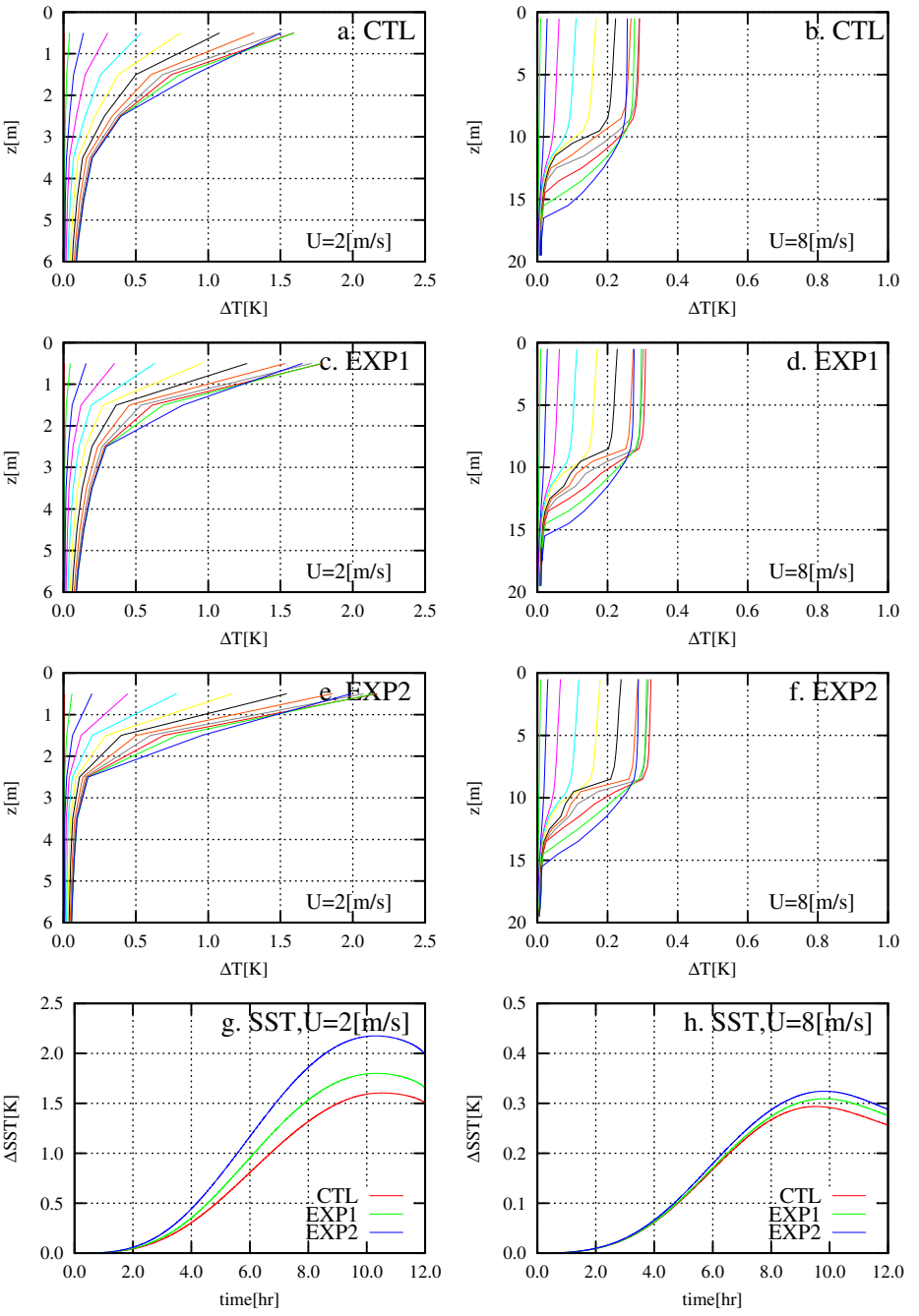

Figure 1. Evolutions of temperature profiles after the onset of surface heating: (a and b) CTL, (c and d) EXP1, and (e and f) EXP2 with different colors denoting profiles in every hour. (g and h) Evolutions of SST after onset of surface heating, with different colors denoting CTL, EXP1, and EXP2. Surface heat flux H is given by $H=H_0[1-\cos(2\pi t/T)]$ with $H_0=350\,\mathrm{W\,m^{-2}}$ and $T=12\,\mathrm{h}$. In Figures 1a, 1c, 1e, and 1g, wind speed is $U=2\,\mathrm{m\,s^{-1}}$. In Figures 1b, 1d, 1f, and 1h, wind speed is $U=8\,\mathrm{m\,s^{-1}}$.

with medium diurnal ranges of less than 1°C, such as in December 1992 and the second half of January 1993. However, CTL underestimates larger diurnal amplitudes of more than 1°C on days with very high insolation and very light winds, especially on 24 October 1992 and around 3 December 1992, when the maximum shortwave flux reached above 950 W/m^2 and the average wind speed was about 1 m/s. On these days, the observed SST diurnal amplitude can reach about 2°C, while that of CTL is only 1°C or less.

Figures 2c–2e compares the mean SST diurnal cycle of each model experiment with observational data. For the entire period, CTL matches the phase of the observations well, but produces amplitude of only 0.3°C,

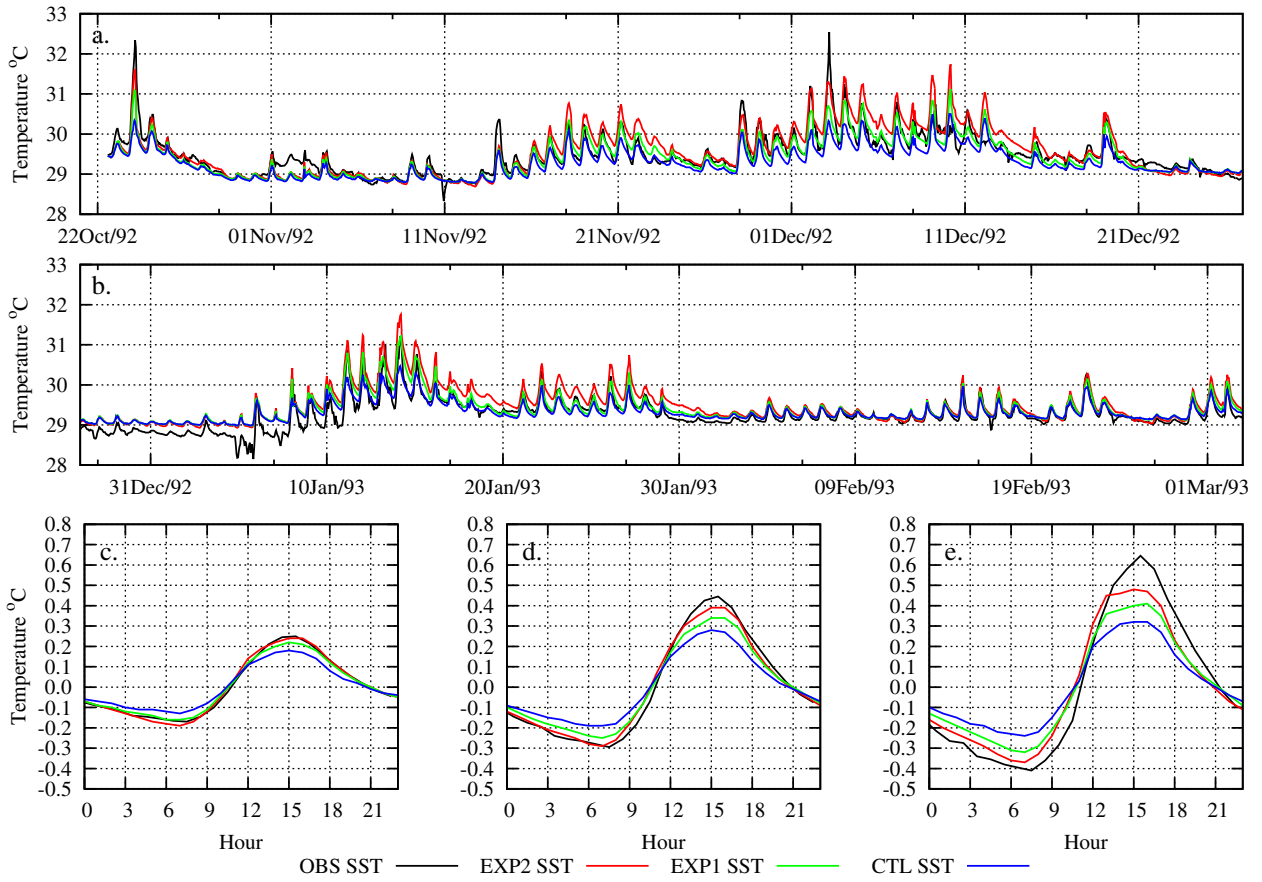

Figure 2. (a and b) Time series of hourly SST observed (black), SST as modeled in the control experiments (CTL, blue), the momentum penetration (EXP1, green), and the momentum plus solar radiation penetration (EXP2, red), and the averaged diurnal cycle of: (c) all days, (d) days with diurnal amplitude great than 0.5°C, and (e) days with diurnal amplitude great than 1°C.

which is 70% of the observed 0.43°C. For the days with diurnal amplitudes larger than 0.5°C, CTL simulates 0.48°, which is 65% of the observed 0.74°C. For the days with diurnal amplitudes greater than 1.0°C, the model produces 0.56°C, which is 53% of the observed 1.05°C. Thus, CTL can only capture about half of the diurnal amplitude in most cases.

Note that there are many observed SST records with large diurnal amplitudes. During the 128 day IMET observation period, there were 55 days (∼43%) with diurnal amplitudes greater than 0.5°C, and 22 days (∼17%) with amplitudes greater than 1.0°C. A similar statistic occurred in the NDBC observations (see below). Hence, large diurnal SST variations occur quite often, and the original model's significant underestimation of these conditions is a major concern. This is the motivation for incorporating these improvements, the effects of which are presented below.

4.2.2. Momentum Penetration

EXP1, which adds the momentum penetration scheme of *Zhang and Zebiak* [2002], does not significantly change the seasonal SST variation from that of CTL. EXP1 and CTL agree closely on days with lower shortwave (below 800 W/m^2 in most records) and higher wind speed (average above 5 m/s), such as from 20 December 1992 to 6 January 1993 and 1–15 February 1993. During calm and sunny days, EXP1 produces larger (and so more realistic) diurnal amplitudes due to the increased stability that keeps more heat content in the topmost layers. As shown in Figure 2, the average diurnal amplitude of EXP1 is 0.37°C, which is 0.07°C (23%) larger than that of CTL throughout the whole period. EXP1 enhances the CTL diurnal cycle by 0.11°C during the days with amplitude larger than 0.5°C, and by 0.16°C (30%) during the days with amplitude greater than 1.0°C. Thus, the momentum penetration helps capture the SST diurnal cycle more realistically, improving the amplitude by about 20–30%.

4.2.3. Solar Penetration

In both CTL and EXP1, the solar penetration scheme was based on the nine-band model [*Paulson and Simpson*, 1981; *Soloviev and Schlüssel*, 1996] with *Jerlov* [1976] water type II. EXP2, incorporating the new

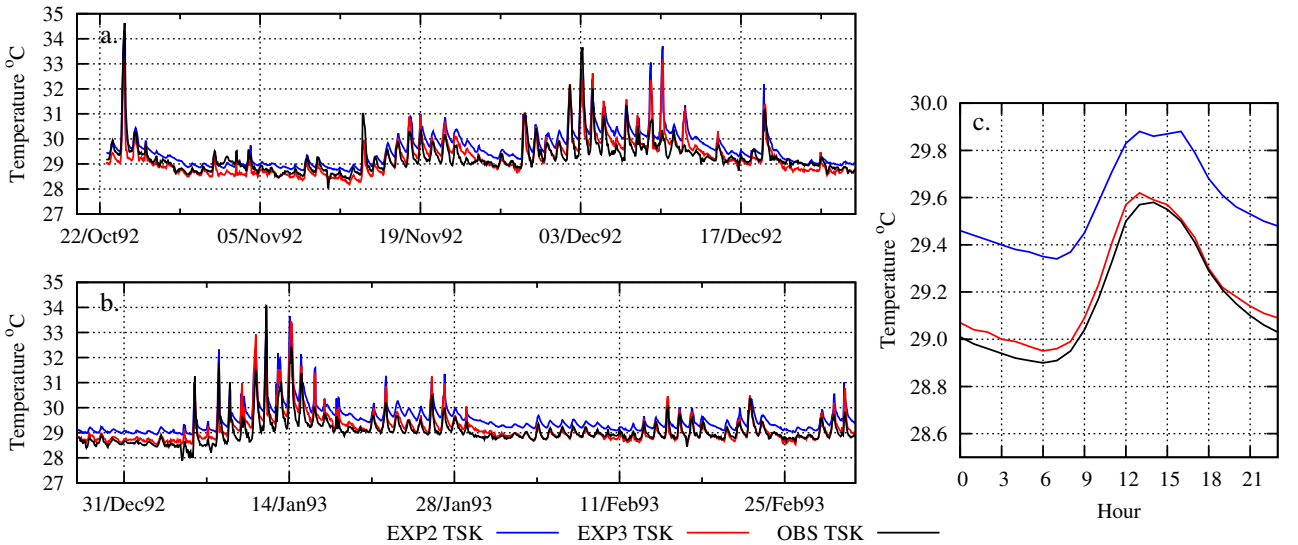

Figure 3. (a and b) Time series of hourly TSK analyzed (black) and simulated in the control experiments (EXP2, blue) and the cool-skin effect experiments (EXP3, red), and (c) the average diurnal cycle of TSK comparison.

penetration scheme of *Kara et al.* [2005], does not significantly change the SST seasonal variation (Figure 2), especially on windy days with lower insolation, such as days late in December 1992 and February 1993. But the new scheme obviously increases the magnitude during days with significant diurnal amplitude, such as 24 October 1992, late November 1992, and early December 1992. As shown in Figure 2, EXP2 diurnal amplitude reaches an average of 0.43°C over the period, which matches very well with the observed 0.44°C. EXP2 reduces EXP1 diurnal cycle bias by 0.09°C (15%) and 0.12°C (17%) on days with amplitudes greater than 0.5°C and 0.1°C, respectively.

4.2.4. Cool-Skin Temperature

In EXP2, *Noh et al.* [2011] used the warm-layer algorithm of *Zeng and Beljaars* [2005] in TSK calculation, but did not consider cool-skin effects on TSK in that scheme. In contrast, EXP3 considers both cool-skin and

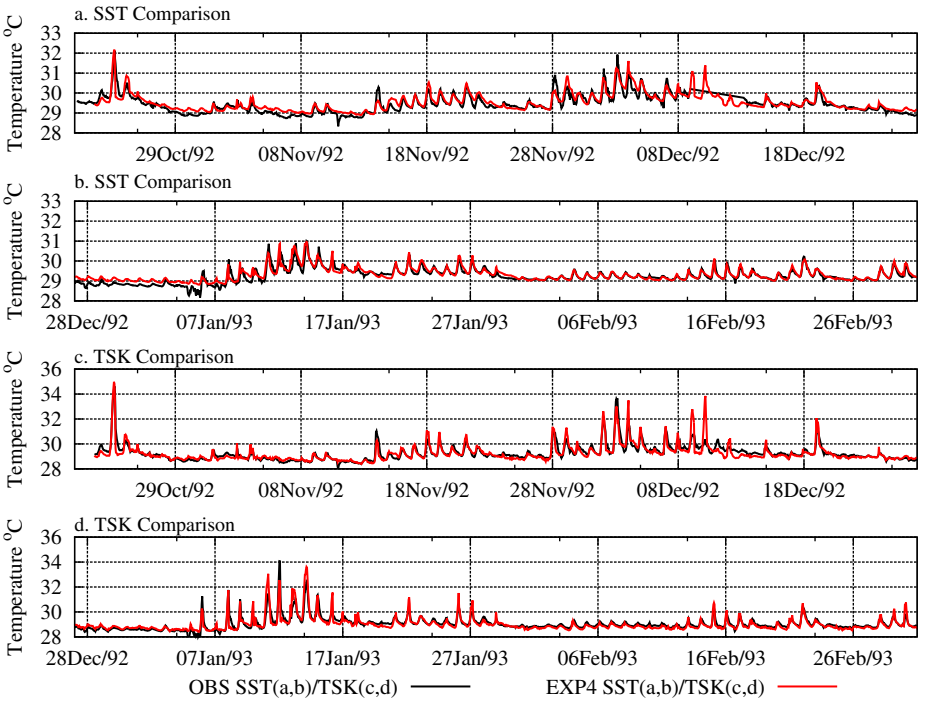

Figure 4. Time series of hourly observed SST and TSK (black) compared with the modeled SST and TSK (label EXP4, red).

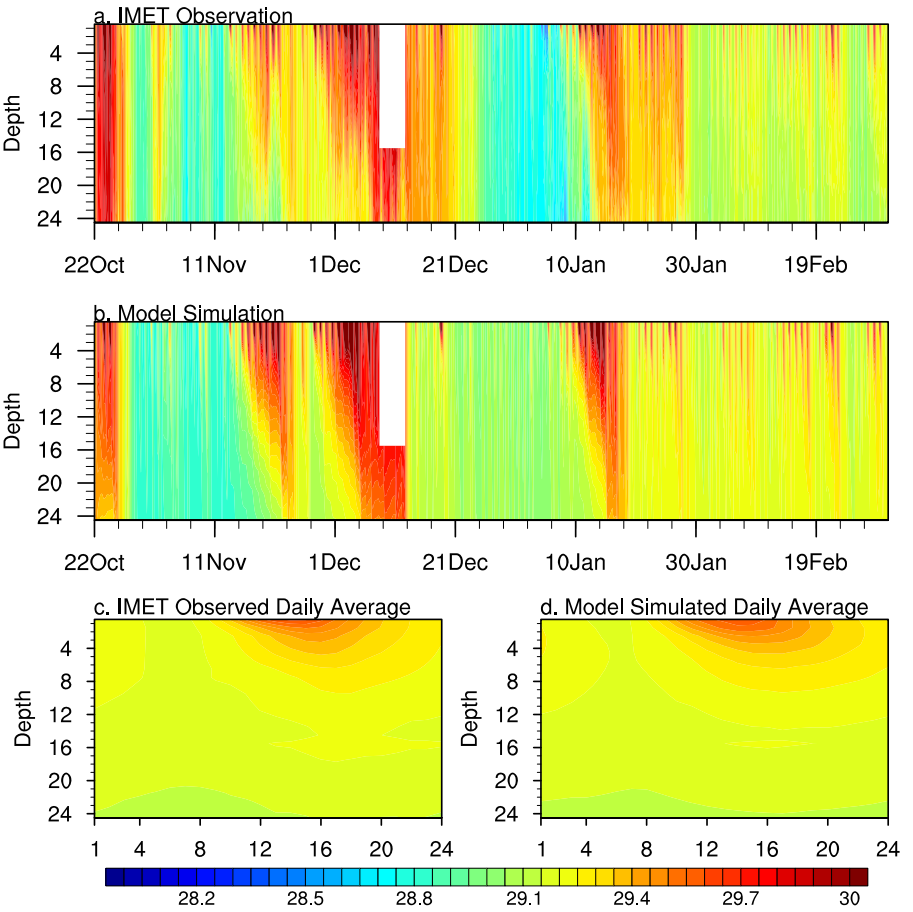

Figure 5. Temperature slice comparison between (b and d) EXP3 and (a and c) IMET observations over the whole simulation period (Figures 5a and 5b) and the daily average (Figures 5c and 5d).

warm-layer effects, thus simulating the TSK variation more realistically throughout the whole period (Figures 3a and 3b). The diurnal amplitude is larger for TSK than for SST, with respective averages of 0.67°C and 0.43°C. The cool-skin effect reduces the model's systematic warm bias by 0.4°C (60%) in the average diurnal cycle (Figure 3c). It also enhances the average TSK diurnal amplitude from 0.53°C in EXP2 to 0.66°C in EXP3.

4.2.5. Numerical Improvement

EXP4 incorporates the vertical grid stretch and the daily SST nudging together with the semi-implicit time integration using $\beta = 0.4$ and $\Delta t = 120$ s, and initializes the model with a homogeneous profile of the observed SST. Compared to EXP3, which uses 150 levels and a time step of 60 s, EXP4 uses 30 levels and consumes only 1/24 of the CPU time. Yet as shown in Figure 4, EXP4 performs as well as EXP3 for both the seasonal evolution and diurnal cycle. This is essential for coupling the mixed layer model with a climate model like CWRF [*Liang et al*., 2012], where both system memory allocation and computing demand are important concerns in long-term simulations.

4.2.6. Mixed-Layer Simulating Evaluation

A reasonable vertical structure is among the most essential indicators of model performance. The EXP3 simulations of sea temperature (Figure 5a) and its averaged diurnal cycle (Figure 5c) as a function of depth and time were compared with IMET observations (Figures 5b and 5d, respectively). Note that there are no observed temperature data in vertical levels from 8 to 12 December 1992, so the simulations in this period are set to missing value for consistency. In weak wind conditions on days with large SST diurnal amplitude, the model can successfully reproduce the shallow mixed layer, such as the days around 1 December 1992 and 10 January 1993. In strong wind condition on days with small SST diurnal amplitude, the model also can reproduce deep mixed layer very well (Figures 5a and 5b). Comparison of observed and modeled average diurnal cycle(Figures 5c and 5d) shows that the model can successfully reproduce a shallow warm layer formed after sunrise on top of the uniform mixed layer, which gets thicker after noon, and also shows the

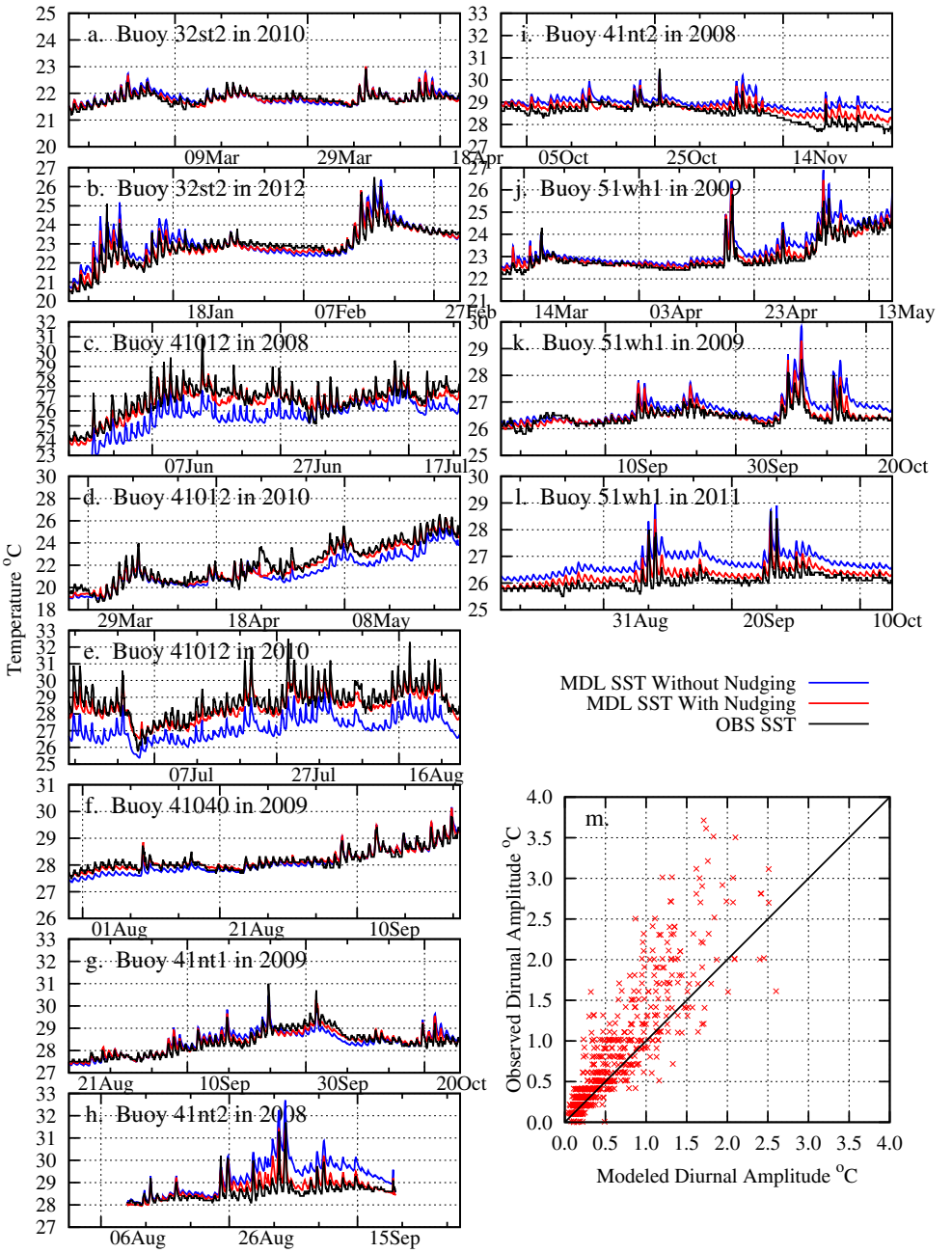

Figure 6. (a–l) Time series of hourly SST variations at the select NDBC buoys, observed (OBS, black) and modeled SST with/without nudging (MDL, red/Blue), and (m) comparison of the SST diurnal amplitude between model and observation.

mixed layer extends to the deeper ocean. Thus, the improvement of SST simulation in this study maintains a reasonable vertical structure.

4.2.7. Independent Evaluation

To test the robustness of the model, another experiment was conducted using the final model configuration, identical to EXP4 but using NDBC buoys along the U.S. coastal oceans. Figure 6 compares the modeled and observed SST variations for five select buoys, both with and without SST nudging. (Every temperature series in Figures 6a–6l is a selected section of the whole simulation period, in order to show diurnal variation clearly). There were about 800 days split into 12 periods for buoy stations 32st2, 41012, 41040, 41nt1, and 51wh1, which were located from 14°N to 30°N and from 85°W to 157°W. The average SST diurnal amplitude of all the records is 0.5°C. About half of these records had SST diurnal amplitude larger than 0.5°C, and more than one quarter (201 days) were greater than 1.0°C.

SST nudging reduces long-term trend bias by more than 2°C in the simulation of buoy 41012 (Figures 6c–6e). Buoy 41012 was located at 30.042°N, 80.534°W around the path of the Gulf Stream, which is a powerful, warm, and swift Atlantic ocean current with a typical maximum speed of about 2.5 m/s. Since ocean currents (except tidal currents) are a continuous factor without a significant diurnal cycle, they do not much impact the SST diurnal variation. The rest of the buoys shown in Figure 6 were not around strong currents, so horizontal advection does not affect temperature trend evolution. Thus, the one-dimensional model works well without SST nudging.

The model reproduces the observed SST long-term variations well (Figures 6a–6l). However, its simulated SST diurnal amplitude averages to only 0.4°C, which is 20% smaller than that of the observations. Figure 6m compares the simulated diurnal amplitude with the observed values. The model clearly underestimates the SST diurnal amplitude. In cases where the diurnal amplitude is smaller than 1°C, the model is quite realistic. However, as the amplitude increases, the degree of model underestimation grows. In cases where the amplitude is greater than 2.5°C, the model does not perform as well as in the IMET-driven experiments above. In these cases (∼20 days, or 3% of all simulated days), the observed SST always exhibits a rapid rise of 1–2°C within 3 h, reaching the peak after slowly warming in the morning. The model fails to resolve such a rapid rise. This failure may be because the data from the NDBC buoys are not as high quality or complete as that from IMET. Since NDBC provides no high-frequency data for the key forcing variables (surface wind stress, latent and sensible heat fluxes, and net longwave radiation), the parameterization schemes from CWRF [*Liang et al*., 2012] were used to derive their estimates, which could introduce large biases. Complete observations with higher quality and frequency, as in the IMET data, are required to understand the SST rapid rise process and its link to air-sea flux exchanges, and thereby to explain (and hopefully overcome) the model's inability to simulate some large amplitudes of SST diurnal cycles.

5. Summary and Conclusion

The upper ocean mixed layer model developed in this study simulates the diurnal cycle of SST and TSK extremely well. The model is based on the TKE closure scheme [*Noh*, 1996; *Noh and Kim*, 1999; *Noh et al*., 2004, 2011]. The improvements include the incorporation of a momentum penetration scheme, a radiation penetration scheme, a cool-skin temperature scheme, and a semi-implicit time integration scheme, along with a vertical grid stretch and a mean SST nudging algorithm. These modifications improved the new model's simulation of SST and TSK diurnal variation, and consequently its match with observations. The model has also been reengineered to improve computational efficiency and portability so that it may be coupled with an ocean and/or atmosphere model. In fact, it has already been coupled with the regional climate model CWRF [*Liang et al*., 2012]. The effects of such coupling on regional climate simulations will be topic for future consideration.

The new model was validated against observations from the IMET mooring data from TOGA-COARE in the tropics, and also independently with data from the NDBC buoys along the U.S. coastal oceans in the extratropics. The model reproduces the SST and TSK diurnal cycle well in both phase and magnitude. The skill improvement over the original model is significant, especially in cases with large diurnal amplitudes. In the IMET data, 43% of the records had diurnal amplitudes larger than 0.5°C, while 17% were greater than 1°C. The NDBC data showed even larger percentages, with 50% and 25% records, respectively. This demonstrates the importance of realistically resolving the SST diurnal cycle, as is achieved in this model. Therefore, in the future, it will be imperative to more realistically resolve the SST diurnal cycle, especially in large amplitude cases, such that air-sea interaction and its climate impact can be appropriately represented in the coupled atmosphere-ocean models. Further improvements to the model developed here are needed to better capture SST diurnal cycles with amplitudes greater than 2°C, although more comprehensive and more frequent in situ observations of surface fluxes are necessary to better understand the model behavior.

SST and TSK diurnal cycles impact regional climate through air-sea interaction, and potentially affect atmospheric circulation at larger scales. These effects are associated with significant variations in evaporation, sensible heat, and other surface fluxes, and also change the strength and pathway of moisture transfer from the ocean to land [*Li et al*., 2001; *Shinoda*, 2005], therefore, eventually affecting climate variations at longer time scales. These will be investigated using this new upper ocean mixed layer model coupled with the CWRF [*Liang et al*., 2012].

Appendix A

A two-band scheme developed by *Kara et al*. [2005] was applied in this study. This scheme makes the radiation attenuation a special continuous quantity that can be derived and retrieved by satellite data such as Sea-Viewing Wide Field-of-View Sensor (SeaWiFS) data for the spectral diffuse attenuation coefficient at 490 nm. The scheme is parameterized as $\frac{Q_{sol}(z)}{Q_{sol}(0)} = (1-\gamma)\exp\left(\frac{-z}{0.5}\right)+\gamma\exp\left(-z\kappa_{PAR}\right)$, where $Q_{sol}(z)$ is the total shortwave radiation at depth z, κ_{PAR} is the attenuation of photosynthetically active radiation (PAR), and $\gamma = \max\left(0.27, 0.695-5.7\kappa_{PAR}\right)$ is the proportion of the spectrum irradiance (primarily in blue) to total incident irradiance. In order to facilitate comparison with the work of *Noh et al*. [2011] on the base model, this study sets $\kappa_{PAR}=0.12\,\mathrm{m}^{-1}$ (i.e., $d1 = 0.5$ m, $d2 = 8.3$ m in double exponential formulation mentioned before) roughly corresponding to Jerlov water type II turbidity [*Kara et al*., 2005]. However, $d1$ and $d2$ are much smaller, which helps the upper ocean keep about 7% more heat from the surface to depths of 3 m, but still maintain the same heat from the surface to depths of 15 m.

Acknowledgments
The observed data of this study are available from Woods Hole Oceanographic Institution (http://www.whoi.edu/) and National Data Buoy Center (http://www.ndbc.noaa.gov). This work was jointly supported by the NOAA Education Partnership Program COM Howard 00073421000037534, National Science and Technology Infrastructure Program (the 12th Five-Year Plan) under grant 2012BAC19B08 in China, the National Natural Science Foundation of China grant 41376016, and Special Fund for Marine Research in the Public Interest 201205018-2. And we acknowledge two anonymous reviewers for their constructive comments and suggestions for improving the manuscript.

References

Anderson, S. P., R. A. Weller, and R. B. Lukas (1996), Surface Buoyancy forcing and the mixed layer of the Western Pacific warm pool: Observations and 1D model results, *J. Clim.*, *9*(12), 3056–3085.
Bernie, D., S. Woolnough, J. Slingo, and E. Guilyardi (2005), Modeling diurnal and intraseasonal variability of the ocean mixed layer, *J. Clim.*, *18*(8), 1190–1202.
Bernie, D., E. Guilyardi, G. Madec, J. Slingo, and S. Woolnough (2007), Impact of resolving the diurnal cycle in an ocean–atmosphere GCM. Part 1: A diurnally forced OGCM, *Clim. Dyn.*, *29*(6), 575–590.
Bernie, D., E. Guilyardi, G. Madec, J. Slingo, S. Woolnough, and J. Cole (2008), Impact of resolving the diurnal cycle in an ocean–atmosphere GCM. Part 2: A diurnally coupled CGCM, *Clim. Dyn.*, *31*(7-8), 909–925.
Chen, D., L. M. Rothstein, and A. J. Busalacchi (1994), A hybrid vertical mixing scheme and its application to tropical ocean models, *J. Phys. Oceanogr.*, *24*(10), 2156–2179.
Chou, S.-H., W. Zhao, and M.-D. Chou (2000), Surface heat budgets and sea surface temperature in the Pacific Warm Pool during TOGA COARE, *J. Clim.*, *13*(3), 634–649.
Clayson, C. A., and A. Chen (2002), Sensitivity of a coupled single-column model in the tropics to treatment of the interfacial parameterizations, *J. Clim.*, *15*(14), 1805–1831.
Clayson, C. A., and L. H. Kantha (1999), Turbulent kinetic energy and its dissipation rate in the equatorial mixed layer, *J. Phys. Oceanogr.*, *29*(9), 2146–2166.
Colbo, K., and R. A. Weller (2009), Accuracy of the IMET Sensor Package in the subtropics, *J. Atmos. Oceanic Technol.*, *26*(9), 1867–1890.
Feng, M., R. Lukas, P. Hacker, R. A. Weller, and S. P. Anderson (2000), Upper-ocean heat and salt balances in the western equatorial Pacific in response to the intraseasonal oscillation during TOGA COARE*, *J. Clim.*, *13*(14), 2409–2427.
Gaspar, P., Y. Grégoris, and J. M. Lefevre (1990), A simple eddy kinetic energy model for simulations of the oceanic vertical mixing: Tests at station Papa and long-term upper ocean study site, *J. Geophys. Res.*, *95*(C9), 16,179–16,193.
Hamilton, G. D. (1986), National Data Buoy Center Programs, *Bull. Am. Meteorol. Soc.*, *67*(4), 411–415.
Jerlov, N. G. (1976), *Marine Optics*, Elsevier Sci., N. Y.
Kantha, L. H., and C. A. Clayson (1994), An improved mixed layer model for geophysical applications, *J. Geophys. Res.*, *99*(C12), 25,235–25,266.
Kara, A. B., H. E. Hurlburt, P. A. Rochford, and J. J. O'Brien (2004), The impact of water turbidity on interannual sea surface temperature simulations in a Layered Global Ocean Model*, *J. Phys. Oceanogr.*, *34*(2), 345–359.
Kara, A. B., A. J. Wallcraft, and H. E. Hurlburt (2005), A new solar radiation penetration scheme for use in ocean mixed layer studies: An application to the Black Sea using a fine-resolution Hybrid Coordinate Ocean Model (HYCOM)*, *J. Phys. Oceanogr.*, *35*(1), 13–32.
Kawai, Y., and A. Wada (2007), Diurnal sea surface temperature variation and its impact on the atmosphere and ocean: A review, *J. Oceanogr.*, *63*(5), 721–744.
Kraus, E. B. (1988), Merits and defects of different approaches to mixed layer modelling, in *Elsevier Oceanography Series*, vol. 46, edited by J. C. J. N. and B. M. Jamart, pp. 37–50, Elsevier, N. Y.
Kukulka, T., A. J. Plueddemann, and P. P. Sullivan (2013), Inhibited upper ocean restratification in nonequilibrium swell conditions, *Geophys. Res. Lett.*, *40*, 3672–3676, doi:10.1002/grl.50708.
Large, W., J. McWilliams, and S. Doney (1994), Oceanic vertical mixing: A review and a model with a nonlocal boundary layer parameterization, *Rev. Geophys.*, *32*(4), 363–403.
Li, W., R. Yu, H. Liu, and Y. Yu (2001), Impacts of diurnal cycle of SST on the intraseasonal variation of surface heat flux over the western Pacific warm pool, *Adv. Atmos. Sci.*, *18*(5), 793–806.
Li, X., C. H. Sui, D. Adamec, and K. M. Lau (1998), Impacts of precipitation in the upper ocean in the western Pacific warm pool during TOGA-COARE, *J. Geophys. Res.*, *103*(C3), 5347–5359.
Liang, X.-Z., et al. (2012), Regional climate–weather research and forecasting model, *Bull. Am. Meteorol. Soc.*, *93*(9), 1363–1387.
Martin, P. J. (1985), Simulation of the mixed layer at OWS November and Papa with several models, *J. Geophys. Res.*, *90*(C1), 903–916.
Mcwilliams, J. C., N. J. Norton, P. R. Gent, and D. B. Haidvogel (1990), A linear balance model of wind-driven, midlatitude ocean circulation, *J. Phys. Oceanogr.*, *20*(9), 1349–1378.
Mellor, G. L., and T. Yamada (1982), Development of a turbulence closure model for geophysical fluid problems, *Rev. Geophys. Space Phys.*, *20*(4), 851–875.
Mosedale, T. J., D. B. Stephenson, and M. Collins (2005), Atlantic atmosphere–ocean interaction: A stochastic climate model–based diagnosis, *J. Clim.*, *18*(7), 1086–1095.
Murtugudde, R., J. Beauchamp, C. McClain, M. Lewis, and A. Busalacchi (2002), Effects of penetrative radiation on the upper tropical ocean circulation, *J. Clim.*, *15*(5), 470–486.
Noh, Y. (1996), Dynamics of diurnal thermocline formation in the oceanic mixed layer, *J. Phys. Oceanogr.*, *26*(10), 2183–2195.

Noh, Y. and H. Fernando (1991), A numerical study on the formation of a thermocline in shear-free turbulence, *Phys. Fluids A*, *3*, 422.
Noh, Y. and H. J. Kim (1999), Simulations of temperature and turbulence structure of the oceanic boundary layer with the improved near-surface process, *J. Geophys. Res.*, *104*(C7), 15,621–15,634.
Noh, Y., C. Joo Jang, T. Yamagata, P. Chu and C. Kim (2002), Simulation of more realistic upper-ocean processes from an OGCM with a new ocean mixed layer model, *J. Phys. Oceanogr.*, *32*(5), 1284–1307.
Noh, Y., H. S. Min and S. Raasch (2004), Large eddy simulation of the ocean mixed layer: The effects of wave breaking and Langmuir circulation, *J. Phys. Oceanogr.*, *34*(4), 720–735.
Noh, Y., E. Lee, D.-H. Kim, S.-Y. Hong, M.-J. Kim and M.-L. Ou (2011), Prediction of the diurnal warming of sea surface temperature using an atmosphere-ocean mixed layer coupled model, *J. Geophys. Res.*, *116*, C11023, doi:10.1029/2011JC006970.
Ohlmann, J. C. (2003), Ocean radiant heating in climate models, *J. Clim.*, *16*(9), 1337–1351.
Ohlmann, J. C., and D. A. Siegel (2000), Ocean radiant heating. Part II: Parameterizing solar radiation transmission through the upper ocean, *J. Phys. Oceanogr.*, *30*(8), 1849–1865.
Paulson, C. A., and J. J. Simpson (1981), The temperature difference across the cool skin of the ocean, *J. Geophys. Res.*, *86*(C11), 11,044–11,054.
Phillips, O. M. (1966), *The Dynamics of the Upper Ocean*, Cambridge Univ. Press, Cambridge, U. K.
Plueddemann, A., R. Trask, W. Ostrom, R. Weller, B. Way, S. Anderson, N. Bogue, J. Shillingford, and S. Hill (1993), TOGA COARE mooring deployment, check-out, and recovery cruises, *Tech. Rep. WHOI-93-50*, Woods Hole Oceanog. Inst., Woods Hole, Mass.
Plueddemann, A. J., and R. A. Weller (1999), Structure and evolution of the oceanic surface boundary layer during the Surface Waves Processes Program, *J. Mar. Syst.*, *21*(1), 85–102.
Price, J. F., R. A. Weller, and R. Pinkel (1986), Diurnal cycling: Observations and models of the upper ocean response to diurnal heating, cooling, and wind mixing, *J. Geophys. Res.*, *91*(9), 8411–8427.
Seo, H., A. C. Subramanian, A. J. Miller, and N. R. Cavanaugh (2014), Coupled impacts of the diurnal cycle of sea surface temperature on the Madden–Julian oscillation, *J. Clim.*, *27*(22), 8422–8443.
Shinoda, T. (2005), Impact of the diurnal cycle of solar radiation on intraseasonal SST variability in the western equatorial Pacific, *J. Clim.*, *18*(14), 2628–2636.
Shinoda, T., and H. H. Hendon (1998), Mixed layer modeling of intraseasonal variability in the tropical western Pacific and Indian Oceans, *J. Clim.*, *11*(10), 2668–2685.
Soloviev, A. V., and P. Schlüssel (1996), Evolution of cool skin and direct air-sea gas transfer coefficient during daytime, *Boundary Layer Meteorol.*, *77*(1), 45–68.
Sui, C.-H., X. Li, K.-M. Lau, and D. Adamec (1997), Multiscale air–sea interactions during TOGA COARE, *Mon. Weather Rev.*, *125*(4), 448–462.
Vitart, F., S. Woolnough, M. Balmaseda, and A. Tompkins (2007), Monthly forecast of the Madden-Julian Oscillation using a coupled GCM, *Mon. Weather Rev.*, *135*(7), 2700–2715.
Weller, R., and S. Anderson (1996), Surface meteorology and air-sea fluxes in the western equatorial Pacific warm pool during the TOGA Coupled Ocean-Atmosphere Response Experiment, *J. Clim.*, *9*(8), 1959–1990.
Weller, R. A., F. Bradley, and R. Lukas (2004), The interface or air–sea flux component of the TOGA coupled ocean–atmosphere response experiment and its impact on subsequent air–sea interaction studies*, *J. Atmos. Oceanic Technol.*, *21*(2), 223–257.
Woolnough, S., F. Vitart, and M. Balmaseda (2007), The role of the ocean in the Madden-Julian Oscillation: Implications for MJO prediction, *Q. J. R. Meteorol. Soc.*, *133*(622), 117–128.
Zeng, X., and A. Beljaars (2005), A prognostic scheme of sea surface skin temperature for modeling and data assimilation, *Geophys. Res. Lett.*, *32*, L14605, doi:10.1029/2005GL023030.
Zhang, R. H., and S. E. Zebiak (2002), Effect of penetrating momentum flux over the surface boundary/mixed layer in az-coordinate OGCM of the tropical Pacific, *J. Phys. Oceanogr.*, *32*(12), 3616–3637.